Analytical Methods

ROYAL SOCIETY OF CHEMISTRY

PAPER

View Article Online
View Journal | View Issue

Cite this: *Anal. Methods*, 2025, **17**, 1900

UPLC-QTOF-MS-based metabolomics and chemometrics studies of geographically diverse *C. torulosa* needles†

Radhika Khanna,* Khushaboo Bhadoriya, Gaurav Pandey and V. K. Varshney*

Cupressus torulosa, an evergreen tree commonly known as the Himalayan or Bhutan cypress, is a significant coniferous species native to the Himalayan regions of Bhutan, northern India, Nepal, and Tibet. In this study, we employed ultra-performance liquid chromatography quadrupole time-of-flight mass spectrometry (UPLC-QTOF-MS) integrated with chemometrics to analyze the metabolite profiles of *C. torulosa* needles collected from 14 distinct geographical regions. Advanced statistical tools, including Principal Component Analysis (PCA) and Hierarchical Cluster Analysis (HCA), were utilized to identify significant variations in the chemical composition across these locations. Our analysis identified 24 marker compounds consistently present in all samples, screened using stringent filtering criteria including One-way ANOVA, moderated *T*-test, and multiple testing correction with the Benjamini–Hochberg FDR method. Additionally, for the first time, we established the flavonoid biosynthesis pathway in *C. torulosa*, enhancing the understanding of its metabolic fingerprint. These findings provide critical insights into the phytochemical diversity of *C. torulosa* and offer valuable tools for quality control, authentication and advancing the application of UPLC-QTOF-MS in natural product research.

Received 7th September 2024
Accepted 31st January 2025

DOI: 10.1039/d4ay01654h

rsc.li/methods

1. Introduction

Cupressus torulosa (*C. torulosa*), commonly referred to as the Himalayan cypress or Bhutan cypress, stands as a distinguished species of cypress indigenous to the Himalayas, specifically inhabiting regions in Bhutan, northern India, Nepal, and Tibet. This evergreen coniferous tree typically reaches heights ranging from 20 to 45 meters (66 to 148 feet) and features a trunk diameter of up to 3 meters (9.8 feet).[1,2] Its form is often conical or columnar, adorned with lush foliage. The foliage showcases dense, dark green scale-like leaves arranged in pairs opposite to each other in a decussate pattern, emitting a unique fragrance when crushed. Adorning the branches are small, spherical cones transitioning from green to brown as they mature, housing diminutive winged seeds within. *C. torulosa* predominantly thrives in mountainous terrains at elevations spanning from 1200 to 3600 meters (3900 to 11 800 feet), favoring well-drained soil and frequently gracing rocky slopes and cliffs.[3,4] Revered within its native habitat, *C. torulosa* often finds itself planted around temples and sacred grounds, boasting cultural significance. Additionally, its timber, prized for construction and fuel, further highlights its value. Although not currently classified as endangered, *C. torulosa* confronts threats stemming from habitat degradation and fragmentation due to human interventions like logging and agriculture. Renowned for its aesthetic appeal and adaptability to diverse soil compositions, *C. torulosa* also finds a place in gardens and parks worldwide as an ornamental tree, showcasing resilience against varying temperatures, drought, and frost once established.[1–5]

The needles of *C. torulosa* are valued for their medicinal properties, including anti-inflammatory, anticonvulsant, antimicrobial, diuretic, stimulant, and antiseptic effects.[6,7] Traditionally, they have been used to treat rheumatism, whooping cough, colds, and wounds, while also serving as astringents and protecting stored grains from insect infestations.[4,8,9] The needles of *C. torulosa* are aromatic, and while extensive research on their volatilomics has been conducted and published worldwide,[10] studies on their non-volatile components are limited. We are among the pioneers in this area of research.

HPLC-DAD assisted chemical characterization of non-volatile components in the needles of *Cupressus* species has been limited to a few studies, focusing on specific species. The flavonoid and biflavonoid profiles of six species, including *Cupressus funebris*, *Cupressus sempervirens*, *Cupressus glabra*, *Cupressus arizonica*, *Cupressus goveniana*, and *Cupressus lusitanica*, have been established, revealing compounds such as cupressuflavone, amentoflavone, robustaflavone, hinokiflavone, methylrobustaflavone, methylamentoflavone, and dimethylcupressuflavone.[11]

Chemistry & Bioprospecting Division, Forest Research Institute, Dehradun 248006, India. E-mail: khannaradhika113@gmail.com; vkvarshney1967@gmail.com

† Electronic supplementary information (ESI) available. See DOI: https://doi.org/10.1039/d4ay01654h

In *C. arizonica Greene*, quercetin 3-*O*-rhamnoside, cupressuflavone, hinokiflavone, amentoflavone, and robustaflavone have been identified, while wild populations of *C. duclouxiana* Hickel in China contained compounds like cupressoside A and B, matairesinoside, dihydrodehydrodiconiferyl alcohol, its rhamnopyranoside derivatives, (–)-isolariciresinol, and its xylopyranoside derivative. Studies on *C. dupreziana* var.*atlantica* have reported amentoflavone, isocryptomerin, cupressuflavone, and hinokiflavone. Similarly, in *C. funebris Endl.*, compounds such as rutin, quercetin 3-*O*-glucoside, quercetin 3-*O*-rhamnoside, kaempferol 3-*O*-rhamnoside, cupressuflavone, amentoflavone, hinokiflavone, and robustaflavone have been observed. Research on *C. nootkatensis* D. Don has highlighted the presence of amentoflavone and its methylated derivatives, including 4′-*O*-methyl-amentoflavone, 4,4′-di-*O*-methyl-amentoflavone, and 7,4′-di-*O*-methyl-amentoflavone, alongside cupressuflavone, hinokiflavone, and robustaflavone.[12]

We previously reported metabolic profiling of needles of *C. torulosa* based on ultra-performance liquid chromatography quadrupole time-of-flight mass spectrometry (UPLC-QTOF-MS) along with investigations on their biological properties.[4] However, variability of the non-volatile constituents in the needles collected from *C. torulosa* trees grown in different environmental zones is not known. In this study, for the first time, UPLC-QTOF-MS integrating chemometrics was applied for metabolite profiling and discrimination of *C. torulosa* from 14 different geographical locations. Furthermore, we identified previously unknown non-volatile marker compounds in *C. torulosa*, using various statistical tools.

2. Materials and methods

2.1. Plant materials

Needle samples of *C. torulosa* growing in 14 different locations across Indian states were collected, with 13 from Uttarakhand (U K) and 1 from Himachal Pradesh (HP) (Table 1 ESI†). The sample from Himachal Pradesh was selected as it represents a distinct geographical and altitudinal region where *C. torulosa* populations are sparse. These locations are considered distinct based on different geographical, altitudinal, and climatic variations, which are known to significantly influence plant metabolite composition. These criteria ensure a diverse representation of *C. torulosa* populations, enabling a robust chemotypic analysis. An herbarium specimen of the plant consisting of needles and cones was deposited in the Systematic Botany Division's herbarium at the Forest Research Institute (FRI) in Dehradun. Following careful comparison with existing herbarium specimens, a systematic botanist Dr Praveen Verma authenticated the plant, assigning it an Accession number (172 753) for reference.

2.2. Chemicals, and reagents

Hexane, chloroform, and methanol were obtained as LR grade solvents from Merck, India. LC-MS grade methanol and acetonitrile (ACN) were purchased from J. T. Baker, while water and formic acid were obtained from Carlo Erba and Thermo Fisher Scientific, respectively.

2.3. Sample preparation

The *C. torulosa* extraction followed our previous method.[4] The needle samples were subjected to lyophilization at −40 °C for 3 days to ensure thorough drying, following which they were milled using a clean and dried stainless-steel blade grinder, ensuring no risk of leachables or contamination, and stored at −20 °C for further analysis. Moisture content was assessed using a Sartorius moisture meter, ranging from 3–8%. Subsequently, the samples underwent defatting *via* ultrasonication (GT Sonic) with hexane, followed by sequential extraction with chloroform and 25% (w/v) aqueous methanol (AM). In each case plant material to solvent ratio used was of 1 : 10. Each extract was filtered through Whatman no. 1 filter paper. The filtrates were then concentrated using a rotary evaporator (Buchi, Switzerland) at 5 to 6 rpm and temperatures of 30 °C (hexane), 40 °C ($CHCl_3$), and 60 °C (AM), resulting in dark greenish hexane, chloroform, and gummy brownish-black color AM extracts, respectively. Only the AM extracts were retained for further study, while the hexane and chloroform extracts were discarded. The AM extracts were further diluted in LCMS grade methanol and then filtered using 0.22 μm, nylon filter into a 2 mL autosampler UPLC vial to prepare the samples for their UPLC-QTOF-MS analysis.

2.4. UPLC-QTOF-MS analysis

The AM extract was analyzed *via* UPLC-QTOF-MS (Agilent Technologies, USA) using non-targeted metabolomics in negative ion mode. The system comprised a 1290 Infinity II UPLC and a 6546 QTOF-MS, with a ZORBAX RRHD Eclipse Plus C18 column (2.1 × 100 mm, 1.8 μm) maintained at 35 °C. The mobile phases were used 0.1% formic acid in water (Solvent A) and 100% methanol (Solvent B). Chromatographic separation was performed using a gradient elution program: 5% B from 0 to 2 minutes, transitioning to 5–30% B from 2 to 8 minutes, 30–45% B from 8 to 16 minutes, 45–95% B from 16 to 25 minutes, and then decreasing to 5% B from 25 to 30 minutes, followed by a 2 minute post-run time. The flow rate was set at 0.4 ml min^{-1}, and the injection volume was 5 μl.

LCMS data were acquired using Agilent jet spray (AJS) electrospray ionization (ESI†) source in negative ionization modes following the optimized parameters: a capillary voltage (V_{cap}) of 3500 V was applied, with a drying gas temperature set at 320 °C and flow was maintained at 8L min^{-1}, while the nebulizer gas pressure was set 35 psi. The sheath gas temperature was set to 350 °C, with a flow rate of 11 L min^{-1}. A fragmentor voltage of 100 V and collision energy values of 10 V, 20 V, and 40 V were utilized. The acquisition mass range (m/z) was set from 100 to 1500, with an acquisition rate of 3 spectra per second, equivalent to 333.3 MS per spectrum.

The sequence included solvent blanks (LC MS-grade methanol), experimental samples (AM extracts), and QC (sample of pooled samples of all 14 locations). The sequence commenced with three injections of the solvent blank and QC samples to verify and stabilize the UPLC-QTOF-MS system, followed by 12 injections of each location (4 composite sample of each location × 3 replicates each). Additionally, after each set of location

injections, a QC sample and blank sample were run. In total, 202 samples were analysed throughout the experiment. Auto-calibration checks during the sample runs utilized masses 322.0481 and 922.0097 as reference masses.

2.5. Metabolite profiling analysis

The data acquired were analyzed using Agilent Mass Hunter Workstation Data Acquisition sofware version B.03.01 (version 10.0 Qualitative Analysis, Agilent Technologies, Santa Clara, CA, 95 051, USA) to extract molecular features (MFs) from the raw data (.d file) which rely on parameters such as *m*/*z* ratio, ion intensities, isotopic pattern, peak shape and adduct species. An accurate mass threshold of less than 10 ppm was applied. The resulting MFs were tentatively identified by searching MS and MS/MS information against various databases, including METLIN (**http://metlin.scripps.edu/**), Food Database (**http://foodb.ca/**), MassBank (**http://www.massbank.jp/**), and HMDB (**http://hmdb.ca/**). These databases provide lists of possible metabolite identities. Additionally, identification was confirmed by matching observed fragments with reference fragments contained in the above databases.[4]

2.6. Chemometric and statistical analysis

For chemometric and statistical analysis, raw data from 202 LC-MS sample runs underwent batch recursive feature extraction using Agilent Mass Hunter Workstation Profinder version 10.0.2. This process included grouping, alignment, peak picking, normalization, and deconvolution. Subsequently, the data were converted into the.cef file format for import into Mass Profiler Professional software (Agilent Technologies, USA). Candidate chemical ions were filtered using ANOVA (p-value $\leq$ 0.05 and max fold change $\geq$2). A profile plot was generated to visualize various variables within the multivariate dataset.

Different analyses were performed, including Principal Component Analysis (PCA), Hierarchical Cluster Analysis (HCA), and violin plots, scatter plots and box-and-whisker plots were also created. Heatmaps were used to clarify relative quantitative differences among compounds based on their peak intensity. Venn diagrams were used to quantitatively view the compounds. Volcano plots were generated to compare the superior location with other individual locations, using input parameters such as one-way ANOVA, moderated *T*-test, and multiple testing correction with the Benjamini–Hochberg FDR method.

3. Results and discussion

3.1. Putatively identified metabolites in *C. torulosa* needles by UPLC-QTOF-MS

The *C. torulosa* metabolites were separated by UPLC-QTOF-MS and identified by Mass Hunter Workstation software, which resulted in 2964 chemical features detected after peak picking from the mass data obtained in negative mode. These features were further filtered by score >90, ANOVA p value $\leq$ 0.05 resulted in 2057 entities and max fold change $\geq$2 to eliminate false positive ions for the identification which resulted 1944 entities (Fig. 1). Based on our previous in-house chemical library of the

Fig. 1 Vienn diagram representing identified compounds.

genus Cupressus, METLIN and comparing mass spectral data against online databases and published information, a total of 63 compounds were putatively identified: 18 flavonoids, 12 terpenoids, 13 phenols and derivatives, 5 carboxylic acids, 6 heterocyclic compounds, 2 steroids, and 7 miscellaneous compounds (Fig. 1 ESI†). These 63 compounds may necessarily not be present in all populations but are present in the maximum among the 14 populations and are of good abundance. Information including the compound name, molecular formula, adduct *m*/*z*, observed mass, reference mass, mass fragments, identification score, class of compounds, and molecular structures are displayed in Table 2 ESI† and TICs of all 14 populations are displayed in Fig. 2 ESI.† Flavonoids and polyphenols have been reported as the main constituents of *C. torulosa* contributing its health benefits on antioxidant, anti-inflammatory disease prevention.[4]

The findings of this study offer a broader and more representative chemotypic profile of *C. torulosa* compared to previous work.[4] While the earlier publication identified 63 compounds exclusively from the Gopeshwar population, the current study expands this analysis to encompass compounds that are major constituents across multiple populations, signifying broader chemotypic diversity. A total of 42 compounds were reported in the previous study, including methyl 6-*O*-galloyl-beta-D-glucopyranoside, ziprasidone, gallocatechin, 7-deoxyloganate, 3′-glucosyl-2′,4′,6′-trihydroxyacetophenone, 3-methoxysalicylic acid, procyanidin B5, *cis*-3-hexenyl β-primeveroside, fraxin, *p*-coumaroyl quinic acid, verbenalin, cynaroside A, oleoside dimethyl ester, 6-hydroxy-α-pyrufuran, 6-*O*-oleuropeoylsucrose, coniferin, sambacin, diosbulbinoside F, citrusin B, 1,5-dibutyl methyl hydroxy citrate, zizybeoside I, aromadendrin, hyperoside, austalide C, gibberellin A1 glucosyl ester, ethyl 7-*epi*-12-hydroxyjasmonate glucoside, mascaroside, prupaside, naringenin 5-*O*-glucuronide, 3′,7-dimethoxy-4′,5,8-trihydroxyflavone 8-glucoside, cappariloside B, neryl rhamnosyl-glucoside, capsianoside V, theaflavate B, APC, robustaflavone, cupressuflavone, myrsinone, *N*-acetyldopamine, amentoflavone, (±)-12-hydroxy-5,8,10,14-eicosatetraenoic acid (HETE), and phytocassane C. These compounds were re-identified in the current study. Additionally, the current study identified 21 novel compounds that were not previously reported. These include malic acid, shikimic acid, hovenitin I, epigallocatechin, 3,4-dihydroxybenzoic acid, catechin, secoxyloganin, umbelliferone, *m*-coumaric acid, rutin,

apigenin 7-glucoside, 17β-hydroxy-4-mercaptoandrost-4-en-3-one 4-acetate 17-propionate, naringenin, luteolin, pinoquercetin, emodin, 3β-hydroxy-9β-primara-7,15-diene-19,6β-olide, picrasin C, sarcostin, kukoamine D, and L-oleandrosyl-oleandolide. This broader scope provides a more comprehensive understanding of *C. torulosa*'s chemotypic diversity.

Fig. 2 Mass *vs.* RT plot of identified compounds.

Comparing these findings with the studies on other *Cupressus* species, bioactive compounds such as cupressuflavone, amentoflavone, and robustaflavone were also identified in other *Cupressus* species, including *C. funebris*, *C. sempervirens*, *C. glabra*, *C. arizonica*, *C.goveniana*, *C. lusitanica* and *C. arizonica*.[11,12] Additionally, rutin was also reported in *C. funebris* Endl.[12] Other 59 compounds are reported here for the first time in *C. torulosa* highlighting the uniqueness of the current findings and their potential pharmacological relevance.

A profile plot was created to visualize the intensity of detected ions across different geographical locations (Fig. 3 ESI†). This plot helps in understanding the distribution and relative abundance of compounds in a dataset. In LC-MS studies, the mass *versus* retention time (RT) plot is a crucial analytical tool. This plot provides a visual representation of the mass-to-charge ratio (m/z) of detected compounds against their retention time in the chromatographic column. This enables the assessment of compound separation efficiency, detection of co-eluting substances, and facilitates the comparison of chromatographic profiles across different samples (Fig. 2). From the mass *vs.* RT plot it is evident that most of the compound elute at intermediate RT *i.e.* 7–15 minutes moreover the bioactive compounds are also eluting at transitional RT.

Further analyses used Box–Whisker plots (Fig. 4 ESI†) and violin plots (Fig. 3) to visualize the data. Box–Whisker plots summarize data distribution through quartiles, highlighting the spread and skewness of compound measurements across different locations. Violin plots provide a detailed view of the distribution of compound intensities, combining elements of box plots with kernel density plots for comprehensive visualization. Both tools complement each other in LC-MS analysis by offering summary and detailed perspectives of complex datasets.

The box–whisker and violin plots reveal variability in the distribution of compounds across different locations. Locations like Dungar, Gopeshwar, and Munsyari exhibit a high concentration of outliers, while Chirbatya, Munsiyari, Shimla, Vinayak, and Tuneta show a broader range of data, indicated by longer whiskers. In contrast, Suwakholi, Tuneta, and Kanda display less variability with smaller interquartile ranges (IQRs). The Violin plot highlights a higher density of data points in locations like Chakrata and Shimla, reflecting greater consistency in compound intensities. Both plots consistently show Shimla, Munsiyari, and Chirbatya as having higher variability in the central data.

To visualize the differences in the content of these compounds among the fourteen locations, these 63 characterized compounds were displayed as a heatmap (Fig. 4). The heatmap shows that the content of compounds varies from one location to another. Heatmaps are particularly useful for

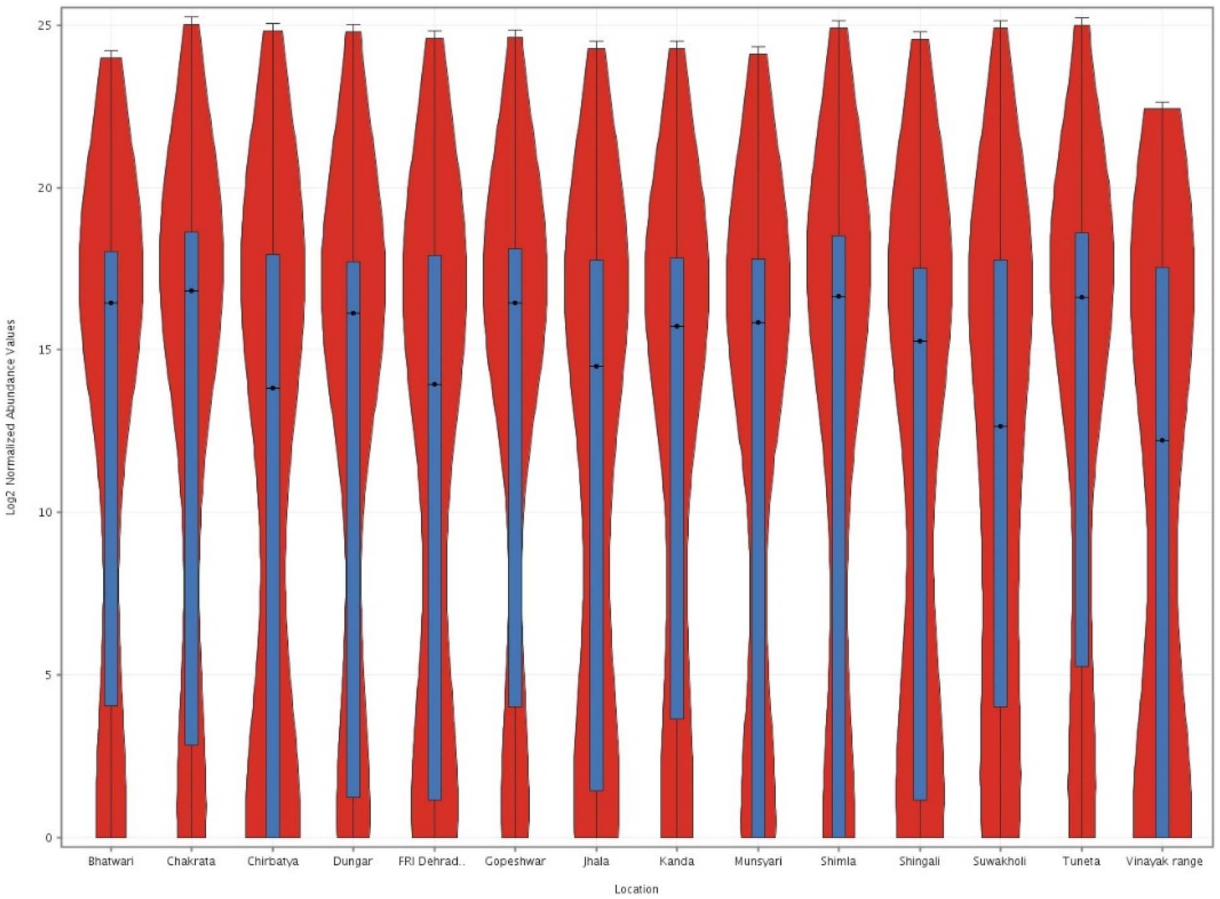

Fig. 3 Voilin plot of identified compounds.

displaying the magnitude of values in a two-dimensional space, making it easier to identify patterns, correlations, and outliers in large datasets. Different color gradients represent the intensities of compounds, with dark red indicating the highest intensity and dark blue indicating the lowest. Cupressoflavone is the most intense compound in all the data set and it is invariably present in all locations where as capsianode V and naringenin 5-*O*-glucuronide are the least abundant compounds.

We also performed Principal Component Analysis (PCA) (Fig. 5) and Hierarchical Cluster Analysis (HCA) (Fig. 6) on our

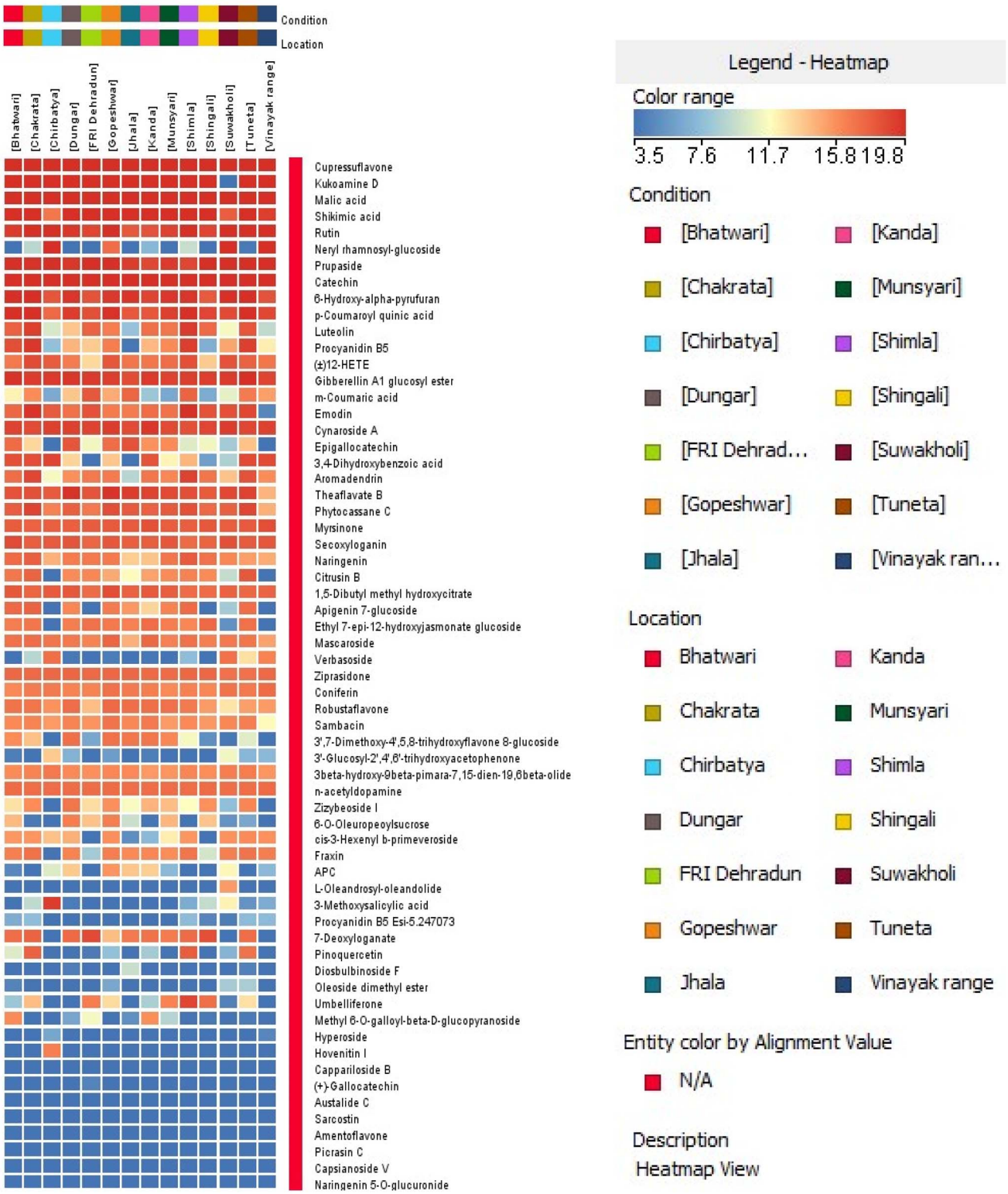

Fig. 4 Heat map of identified compounds.

dataset, which are powerful statistical tools used to analyze and interpret complex datasets. In the PCA analysis, 63 identified compounds were included to investigate primary group differentiations. The PCA analysis utilized predefined species data, and no variable selection was performed by the software.

Fig. 5 Principal component analysis of identified compounds.

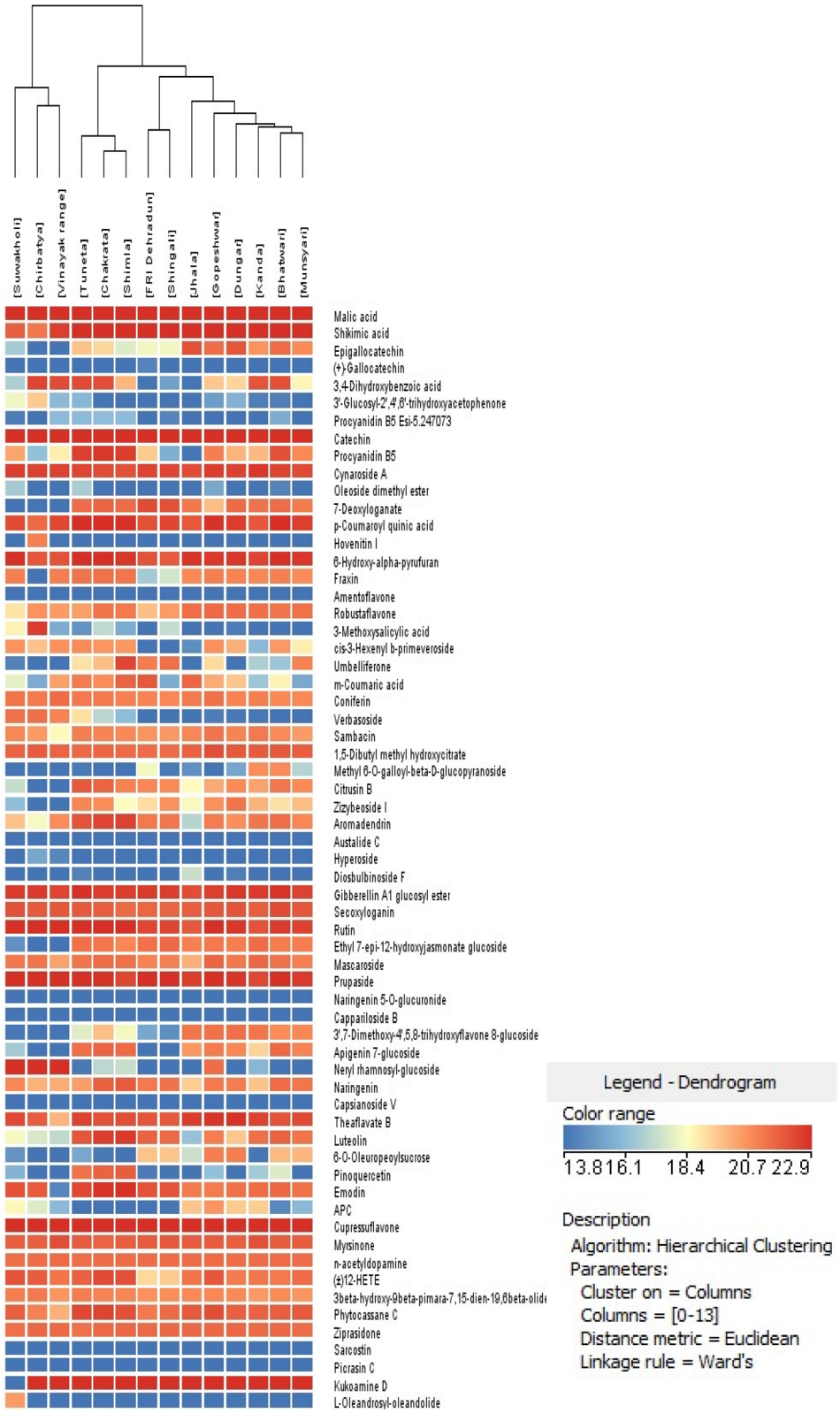

Fig. 6 Hierarchical cluster analysis and dendrogram of identified compounds.

In PCA, the total variance explained by our dataset along the two axes is 50.48% (X-axis = 21.34%, Y-axis = 19.46%, Z axis = 9.68%), which is acceptable for compressed data. The eigenvalues of component 1, component 2 and component 3 are 2.34, 1.94 and 0.968, respectively. Chirbatya, Vinayak and Suwakholi are the three locations that show the maximum variance in the data and are distantly related to all other locations in the terms of chemical variability. Also, the 3D-PCA

plot shows that the QC samples are grouped into a single cluster, indicating the UPLC-QTOF-MS system stability (Purple points, Fig. 5). The clustering of the QC combined samples is distinct and forms a separate group in the PCA plot, positioned away from all individual sample groups, indicating that QC samples are not skewed by any single group. Further, HCA groups locations based on their similarities in compound profiles, creating a dendrogram that illustrates the relationships and distances between clusters. The dendrogram of the HCA plot summarizes the same results illustrated by PCA *i.e.* Chirbatya and Suwakholi are distantly related locations that form a cluster distinct from other locations. Vinayak is the closest location to this cluster.

3.2. Identification of chemotypic marker compounds

In our UPLC-QTOF-MS research, the identification of chemotypic marker compounds plays a pivotal role in characterizing and distinguishing various samples. Chemotypic markers are specific compounds or groups of compounds that characterize *C. torulosa* needles, serving as unique identifiers that reflect the metabolic fingerprint or chemical profile of the needles. By identifying and quantifying chemotypic markers using UPLCQTOFMS, we gain valuable insights into sample composition, variability, and potential biological activity. These markers, reported for the first time in literature for *C. torulosa* needles, can be instrumental in quality control and authentication, contributing to the advancement of fields such as pharmacognosy, natural product chemistry, and metabolomics.

From the initial analysis, 63 compounds were putatively identified based on UPLC-QTOF-MS data and cross-referenced with in-house chemical libraries, METLIN, and other online databases. These compounds represent a preliminary list, capturing the chemotypic diversity across the 14 sampled locations. Subsequently, employing rigorous statistical filtering and conditions stipulating that a compound should be present in all 14 locations and exhibit at least 66% intensity was performed to identify 24 marker compounds. The filtering criteria included a high identification score (>90), statistical significance (ANOVA p-value ≤ 0.05), and a fold change ≥ 2 across locations. A Venn diagram representing the filtration process is shown in Fig. 5 ESI,† while a Mass *vs.* RT plot displaying the arrangement of the compounds according to retention time is depicted in Fig. 6 ESI†. Here also by Mass *vs.* RT plot it is evident that most of the compounds elute at intermediate RT *i.e.* 7 to 15 min. These 24 compounds serve as chemotypic markers for *C. torulosa* and provide critical insights into its metabolic diversity. The transition from the 63 preliminary compounds to the 24 marker compounds highlights the robustness of the statistical workflow employed in this study.

The identified marker compounds are cupressoflavone, malic acid, shikimic acid, rutin, prupaside, catechin, 6-hydroxy-alpha-pyrufuran, *p*-coumaroyl quinic acid, ±12-hete, gibberellin a1 glucosyl ester, cynaroside a, theaflavate b, phytocassane c, myrsinone, secoxyloganin, naringenin, 1,5-dibutyl methyl hydroxycitrate, mascaroside, ziprasidone, coniferin, robustaflavone, sambacin, 3-beta-hydroxy-9-beta-primara-7,15-diene-19,6 beta-*o*-lide and *n*-acetyldopamine. Further, heat map showing the varying intensities of these marker compounds in all the 14 locations is shown (Fig. 7 ESI,† Fig. 7) with cupressoflavone being the chemotypic marker compound with highest intensity whereas malic acid being the second most abundant compound with highest intensity in location Shimla. Additionally, HCA is done on the data and the dendrogram clustering closely related locations is represented in Fig. 7. Here the locations Vinayak, Chirbatya, Suwakholi are closely related and clustered together in the dendrogram.

3.3. Fragmentation pattern of marker compounds and their associated biological activities

Fragmentation pathway of marker compounds, given in Table 2 ESI.†, were also established. Understanding these fragmentation pathways helps in identifying the compounds more accurately during mass spectrometry analysis and can provide insights into their structure and behavior.

Malic acid (RT 0.802, MF $C_4H_6O_5$, m/z 133.0142) undergoes fragmentation to m/z 89.0245 (CO_2 loss) and 71.0133 (H_2O loss) (Fig. 34 ESI†), known for its antibacterial and preservative properties.[13] Shikimic acid (RT 0.819, MF $C_7H_{10}O_5$, m/z 173.0455) generates ions at m/z 155.0353 (H_2O loss), 111.0443 (CO_2 loss), and 72.9934 (diol loss) (Fig. 35 ESI†) and is associated with anti-inflammatory, analgesic, and antibacterial activities.[14,15]

Ziprasidone (RT 2.873, MF $C_{21}H_{21}ClN_4OS$, m/z 411.1063) yields ions at m/z 208.9613 (heteroatomic bond cleavage) and 162.9549 (H_2O along with HCl release) (Fig. 36 ESI†), with antipsychotic and neuroprotective effects.[16,17] *p*-Coumaroyl quinic acid (RT 6.211, MF $C_{16}H_{18}O_8$, m/z 337.0932) breaks into m/z 191.0562 (ester bond cleavage), 163.0402(CO loss), and 119.0459 (CO loss) (Fig. 37 ESI†), attributed to its antioxidant, anti-inflammatory, and anticancer effects.[18,19]

Catechin (RT 6.263, MF $C_{15}H_{14}O_6$, m/z 289.0718) dissociates into m/z 245.0807 (CO_2 loss), 179.0342, and 109.0292 (flavanol ring cleavage) (Fig. 38 ESI†), demonstrating anticancer and antidiabetic activities.[20,21] Secoxyloganin (RT 6.913, MF $C_{17}H_{24}O_{11}$, m/z 403.1226) forms m/z 357.1186 (formic acid release), 179.0528 (glycosidic bond cleavage), and 149.0463 (heterolytic bond cleavage) (Fig. 39 ESI†), with antioxidant, anti-inflammatory, and neuroprotective properties.[22,23]

Cynaroside A (RT 7.124, MF $C_{21}H_{32}O_{10}$, m/z 443.1920) breaks into m/z 219.8699 (volatile molecule release) and 179.0561 (glycosidic bond cleavage) (Fig. 40 ESI†), showing potential against oxidative stress, inflammation, neurodegeneration, and cardiovascular diseases.[24–27] 6-Hydroxy-alpha-pyrufuran (RT 8.217, MF $C_{15}H_{14}O_6$, m/z 289.0717) splits into m/z 109.0296 and 201.0555 (RDA reaction) (Fig. 41 ESI†), active against oxidative stress, microbial infections, and liver diseases.[28–30]

Coniferin (RT 9.353, MF $C_{16}H_{22}O_8$, m/z 341.1239) gives ions at m/z 161.0602 (glycosidic bond cleavage) and 59.0133 (H_2O release), while sambacin (RT 9.568, MF $C_{26}H_{36}O_{12}$, m/z 539.2137) splits into m/z 329.1390 (glycosidic bond cleavage), and 59.0137 (diol loss) (Fig. 42 and 43 ESI†). Both possess antioxidant and anti-inflammatory properties.[31–34]

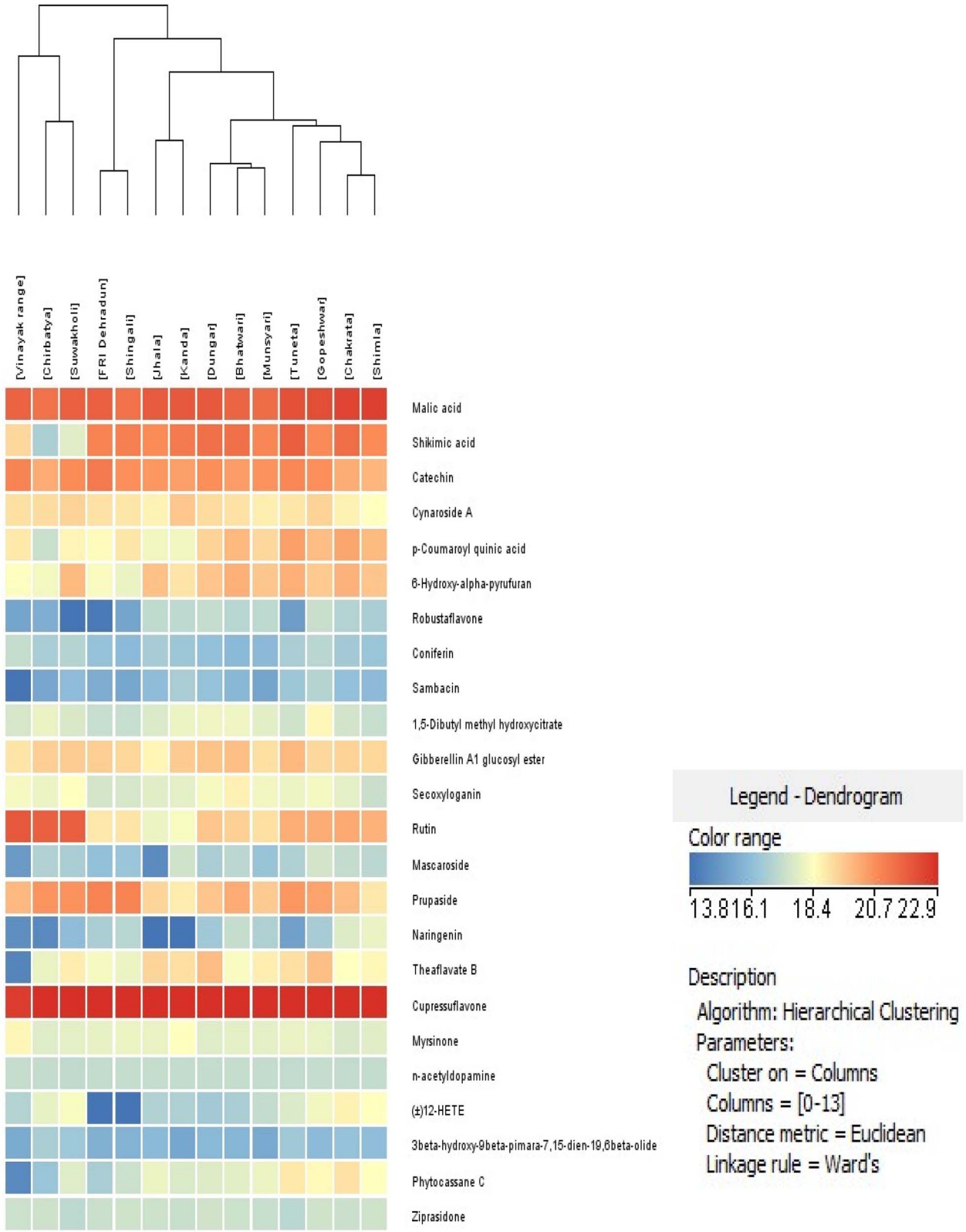

Fig. 7 Hierarchical cluster analysis, dendrogram and heat map of marker compounds.

1,5-Dibutyl methyl hydroxy citrate (RT 10.357, MF $C_{15}H_{26}O_8$, *m*/*z* 333.1553) generates ions at *m*/*z* 234.8990, 175.1022, and 59.0135 (ester bond cleavage) (Fig. 44 ESI†), known for hepatoprotective and anticancer properties.[35,36] Gibberellin A1 glucosyl ester (RT 12.337, MF $C_{25}H_{34}O_{11}$, *m*/*z* 509.2034) releases ions at *m*/*z* 179.0715 and 59.0137 (glycosidic bond and diol loss)

(Fig. 45 ESI†), while rutin (RT 12.457, MF $C_{27}H_{30}O_{16}$, *m*/*z* 609.1431) gives *m*/*z* 343.045 and 178.9976 (glycosidic bond cleavage) (Fig. 46 ESI†). Both act as antioxidants and anti-inflammatory agents.[37–40]

Mascaroside (RT 12.594, MF $C_{26}H_{36}O_{11}$, *m*/*z* 523.2242) produces *m*/*z* 475.1940 (H_2O release), 327.1593 (glycosidic moiety loss), and 133.0271 (methanol and water loss) (Fig. 47 ESI†). Prupaside (RT 13.451, MF $C_{27}H_{36}O_{12}$, *m*/*z* 551.2142) generates *m*/*z* 165.0566 and 375.9805 (glycosidic bond cleavage and methane loss) (Fig. 48 ESI†). Both support neuroprotective and hepatoprotective activities.[41–44]

Naringenin (RT 16.459, MF $C_{15}H_{12}O_5$, *m*/*z* 271.0612) leads to ions at *m*/*z* 243.9003 (CO loss), 151.0035, and 94.9251 (flavonoid ring cleavage) (Fig. 49 ESI†), with cardioprotective effects.[45] Theaflavate B (RT 16.842, MF $C_{36}H_{28}O_{15}$, *m*/*z* 699.1357) forms *m*/*z* 375.0491 (release of phenolic groups) and 257.0093 (heterolytic bond cleavage) (Fig. 50 ESI†), known for anticancer, cardioprotective, and neuroprotective effects.[46–48]

Robustaflavone (RT 19.934, MF $C_{30}H_{18}O_{10}$, *m*/*z* 537.0833) generates *m*/*z* 444.0530 (phenolic molecule loss), 375.051 (RDA reaction), and 331.0613 (diene molecule loss) (Fig. 51 ESI†), with potent antiviral activity against HIV, HSV, and hepatitis B.[49] Cupressuflavone (RT 20.084, MF $C_{30}H_{18}O_{10}$, *m*/*z* 537.0836) breaks into *m*/*z* 443.0407, 417.0314, 375.0512, and 151.0034 (phenolic moiety and ethene release, followed by CO_2 and RDA reaction) (Fig. 52 ESI†). It acts as an antioxidant, anti-inflammatory, and antiviral agent.[50,51]

Myrsinone (RT 21.369, MF $C_{17}H_{26}O_4$, *m*/*z* 293.1759) forms *m*/*z* 236.1049, 221.1540, and 177.0930 (butane, methane, and water release) (Fig. 53 ESI†). *N*-acetyldopamine (RT 21.580, MF $C_{10}H_{13}NO_3$, *m*/*z* 194.0822) releases *m*/*z* 153.1286, 150.9773, and 58.6112 (acetaldehyde, hydrogen, and amide release) (Fig. 54 ESI†).[52,53] Both compounds support neuroprotective and anticancer activities.[54,55] 3-Beta-hydroxy-9-beta-primara-7,15-diene-19,6 beta-*o*-lide (RT 21.702, MF $C_{20}H_{28}O_3$, *m*/*z* 315.0214) leads to *m*/*z* 278.0210 (methane and ethane release) and 209.1129 (strain-induced cleavage with methane loss) (Fig. 55 ESI†), exhibiting anti-inflammatory activity.[56]

(±)12-Hydroxy-5,8,10,14-eicosatetraenoic acid (RT 23.073, MF $C_{20}H_{32}O_3$, *m*/*z* 319.2281) breaks into *m*/*z* 225.2876 and 96.9603 (strain-induced bond cleavage) (Fig. 56 ESI†), showing anti-inflammatory properties.[57–59] Phytocassane C (RT 24.171, MF $C_{20}H_{30}O_3$, *m*/*z* 317.2124) generates *m*/*z* 271.2062 (release of water and methane molecules) and 83.0501 (strain induced bond cleavage) (Fig. 57 ESI†), with antimicrobial and neuroprotective properties.[60,61]

3.4. Comparison of all locations with superior location (Gopeshwar)

Expanding on prior findings that recognized Gopeshwar for its remarkable biological activity, this study positioned it as a key reference point.[4] So, we compared all locations by taking Gopeshwar as a standard, using scatter plots and volcano plots for the analysis. Scatter plots provide a visual representation of the relationship between two variables, enabling the identification of trends, correlations, and outliers within the data. By plotting the intensity of compounds from Gopeshwar against those from other locations, we can clearly visualize the variations in compound profiles and identify significant differences (Fig. 8–20 ESI†). Vinayak and suwakholi are the populations that are most distantly related to population of Gopeshwar as it contains maximum no of outliers. This data also supports data obtained from HCA.

In our UPLC-QTOF-MS volcano plots were employed to identify significantly different compounds between Gopeshwar and other locations. Volcano plots combine measures of statistical significance (*p*-values) and fold-change, providing a clear visualization of the magnitude and reliability of differences in compound abundance. By plotting the negative log of the *p*-value against the log of the fold-change, volcano plots help in pinpointing compounds that exhibit both high significance and substantial changes in concentration. The volcano plot analysis highlighted compounds with significant differences in abundance between Gopeshwar and other locations (Fig. 21–33 ESI†).

This enables a robust identification of potential chemotypic markers and highlights key compounds contributing to the distinct biological activity observed in Gopeshwar compared to other locations.

3.5. Metabolic pathway

Flavonoids are widely distributed secondary metabolites contributing to plant growth and development and having prominent applications in food and medicine. The elucidation of the biosynthetic pathways, has allowed metabolic engineering of plants through the manipulation of the different final products with valuable applications.[62,63]

In our study, a 25% AM extract prepared from the needles of *C. torulosa* was analyzed using UPLC-QTOF-MS. We employed Mass Profinder Professional (MPP) software to identify key metabolic pathways by matching our findings with WikiPathways. This analysis successfully revealed the flavonoid biosynthesis pathway in *C. torulosa*, marking the first report of this pathway in the literature. Here we also included metabolites with score <90 which are not reported in Table 2 ESI.† Here naringenin chalcone act as precursor molecule for synthesis of naringenin which further acts as predecessor for dihyrotricetin and dihydrokaempferol. Further end product kaempferol and dihydromyricetin are the end products of this process formed from dihydrokaempferol. In the second process, eriodictyol chalcone acts as antecedent for eriodictyol which in turn acts as precursor for dihydrotricetin and the final product formed is quercetin. The compounds highlighted in yellow are more important metabolites of this pathway. Here, transcription factors/genes involved in both the processes are chalcone isomerase (CHI), flavonol synthase (FLS), and flavanone 3-hydroxylase (F3H) (Fig. 8).

This pathway is proposed as a flavonoid biosynthesis pathway specific to the extraction and analytical conditions used, but the inclusion of metabolites with scores <90 and reliance on ionization efficiency highlight the need for further validation through complementary techniques such as transcriptomics, enzyme assays, or isotopic labeling to achieve a more comprehensive understanding.

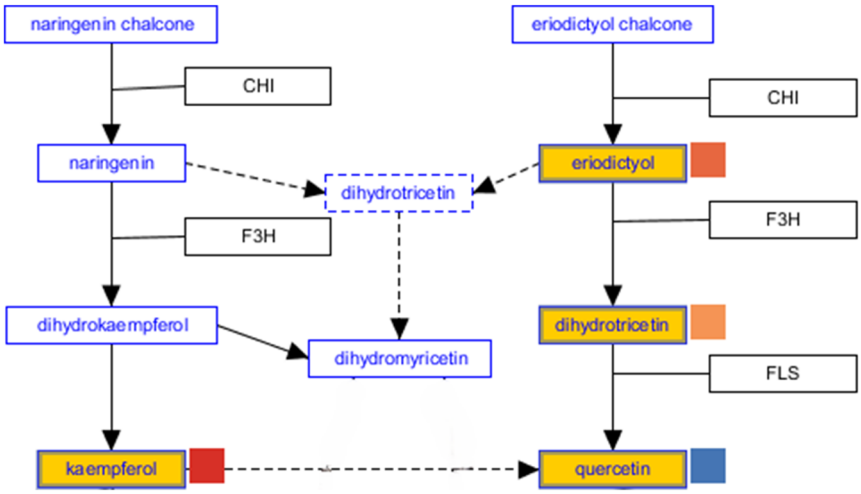

Fig. 8 Flavonoid biosynthesis pathway in *Cupressus torulosa*.

4. Conclusion

In this study, we successfully identified and characterized chemotypic marker compounds from *C. torulosa* needles using UPLC-QTOF-MS. By employing advanced statistical analyses, including Principal Component Analysis (PCA) and Hierarchical Cluster Analysis (HCA), we discerned significant variations in compound profiles across 14 different locations. Stringent filtering criteria enabled the screening of 24 marker compounds, which were consistently present across all locations.

Expanding on prior findings that recognized Gopeshwar for its remarkable biological activity, this study positioned it as a key reference point. Utilizing Gopeshwar as a reference, scatter plots and volcano plots facilitated a detailed comparison, highlighting significant differences to this location. The identification of these chemotypic markers, reported here for the first time, not only enhances our understanding of the metabolic fingerprint of *C. torulosa* needles but also provides valuable tools for quality control and authentication. Further we also tried to establish the flavonoid biosynthesis pathway for *C. torulosa* for the first time in literature.

These findings contribute to the broader fields of pharmacognosy, natural product chemistry, and metabolomics, and offering new insights for the analysis of complex biological samples. Future research can build upon this foundation to explore the bioactivity and therapeutic potential of the identified compounds, further advancing the application of UPLC-QTOF-MS in natural product research.

Abbreviations

25% (w/v) aqueous methanol	AM
Cupressus torulosa	CT
Extracted Ion Chromatogram	EIC
Forest research institute, Dehradun	FRI
Molecular formula	MF
Total Compound Chromatogram	TIC
Ultra-high performance liquid chromatography-quadrupole time of flight – mass spectrometry	UPLC-QTOF-MS
Analysis of variance	ANOVA

Data availability

Data will be made available on request.

Author contributions

Radhika Khanna: collection of data from various online and offline sources and conducting all phytochemical, pharmacological and UPLCQTOFMS experiments, data analysis and writing the original draft of the manuscript; Dr V. K. Varshney: funding acquisition, planning and designing of all phytochemical experiments including UPLCQTOFMS experiments; overall guidance, final drafting and editing of manuscript; Khushaboo Bhadoriya: conducting UPLCQTOFMS analysis experiments; Gaurav Pandey: statistical analysis and data interpretation.

Conflicts of interest

The authors declare that they do not have any conflict of interest regarding the publication of this manuscript.

Acknowledgements

The authors express their gratitude to the Director of the Forest Research Institute, Dehradun, for providing necessary facilities for conducting this work. Financial support from the National Authority CAMPA, Ministry of Environment, Forests & Climate Change, Govt. Of India, to the Indian Council of Forestry Research & Education (ICFRE), Dehradun for the project "Bio-prospecting for Industrial Utilization of Lesser-Known Forest

Plants" under the scheme "Strengthening Forestry Research for Ecological Sustainability and Productivity Enhancement." is gratefully acknowledged. Thanks are also due to the ICFRE to facilitate the successful execution of this research.

References

1 N. Prodr and Fl Nepal, *Cupressus torulosa*, Himalayan cypress, *The Trees Of Great Britain And Ireland*, 1825, vol. 699, pp. 1158–1161.

2 H. Lohani, G. Gwari, H. C. Andola, U. Bhandari and N. Chauhan, α-Pinene rich volatile constituents of *Cupressus torulosa* D. Don from Uttarakhand Himalaya, *Indian J. Pharm. Sci.*, 2012, **74**, 278–280, DOI: **10.4103/0250-474X.106078**.

3 H. Lohani, A. Kumar, U. Bhandari, S. Z. Haider, S. Singh and N. Chauhan, Effect of seasonal and tree girth size variation on *Cupressus torulosa* D. Don leaves essential oil composition growing in Uttarakhand, *J. Essent. Oil Bear. Plants*, 2014, **17**, 1257–1267, DOI: **10.1080/0972060X.2014.998721**.

4 R. Khanna, H. R. Chitme, K. Bhadoriya, Y. C. Tripathi and V. K. Varshney, *In vitro* and *in vivo* anti-inflammatory activity of *Cupressus torulosa* D.DON needles extract and its chemical characterization, *J. Ethnopharmacol.*, 2023, **314**, 116578, DOI: **10.1016/j.jep.2023.116578**.

5 R. Khanna, H. R. Chitme, K. Bhadoriya and V. K. Varshney, *Cupressus torulosa*, a Source of Antioxidant Polyphenols: An Analytical and Pharmacological Study, *Rapid Commun. Mass Spectrom.*, 2025, **39**(3), e9945, DOI: **10.1002/rcm.9945**.

6 S. Gupta, M. Bhagat and R. Sudan, Analysis of chemical composition of *Cupressus torulosa* (D.Don) essential oil and bioautography guided evaluation of its antimicrobial fraction, *Indian J. Exp. Biol.*, 2018, **56**, 252–257. **https://www.researchgate.net/publication/324684731**.

7 D. Sharma, A. Pramanik and P. K. Agrawal, Evaluation of bioactive secondary metabolites from endophytic fungus *Pestalotiopsis neglecta* BAB-5510 isolated from leaves of *Cupressus torulosa* D.Don, *Biotech*, 2016, **6**, 210, DOI: **10.1007/s13205-016-0518-3**.

8 R. C. Padalia, R. S. Verma, A. Chauhan and C. S. Chanotiya, Chemical composition of essential oils of *Cupressus* species, *J. Essent. Oil Res.*, 2013, **25**(4), 251–256.

9 S. Gupta, M. Bhagat, R. Sudan, S. Rajput and K. Rajput, Analysis of chemical composition of *Cupressus torulosa* essential oil and bioautography guided evaluation of its antimicrobial fraction, *Indian J. Exp. Biol.*, 2018, **56**(4), 252–257.

10 P. Bhalla, K. Chauhan and V. K. Varshney, Unveiling geographical variation and chemotypes of *Cupressus torulosa* needles essential oil: A novel approach using *t*-SNE and HCA, *Flavour Fragrance J.*, 2024, **39**, 3816, DOI: **10.1002/ffj.3816**.

11 A. Romani, C. Galardi, P. Pinelli, N. Mulinacci and D. Heimler, HPLC quantification of flavonoids and biflavonoids in *Cupressaceae* leaves, *Chromatographia*, 2002, **56**(7–8), 469–474, DOI: **10.1007/BF02492011**.

12 C. Frezza, D. de Vita, F. Sciubba, C. Toniolo, L. Tomassini, M. Nicoletti, M. Franceschin, M. Guiso, A. Bianco, M. Serafini and S. Foddai, There is not only *Cupressus sempervirens* L.: A review on the phytochemistry and bioactivities of the other *Cupressus* L. species, *Appl. Sci.*, 2022, **12**(14), 7353, DOI: **10.3390/app12147353**.

13 D.-W. Sun, *Emerging Technologies for Food Processing*, Elsevier Academic Press, 2005.

14 D. C. Díaz-Quiroz and C. S. Cardona-Félix, Synthesis, biological activity, and molecular modelling studies of shikimic acid derivatives as inhibitors of the shikimate dehydrogenase enzyme of Escherichia coli, *Bioorg. Med. Chem.*, 2018, **26**, 1801–1809, DOI: **10.1080/14756366.2017.1422125**.

15 J. Y. Sun, C. Y. You, K. Dong and H. S. You, Anti-inflammatory, analgesic, and antioxidant activities of 3,4-oxo-isopropylidene-shikimic acid, *Pharm. Biol.*, 2016, **54**, 1428–1435, DOI: **10.3109/13880209.2016.1153663**.

16 C. F. Caley and C. K. Cooper, Ziprasidone: the fifth atypical antipsychotic, *Ann. Pharmacother.*, 2002, **36**, 1114–1122, DOI: **10.1345/aph.1A053**.

17 K. Terada, A. Murata, E. Toki, S. Goto and H. Yamakawa, Atypical antipsychotic drug ziprasidone protects against rotenone-induced neurotoxicity: An *in vitro* study, *Molecules*, 2020, **25**, 4206, DOI: **10.3390/molecules25184206**.

18 Y. Zhang, X. Zhang, Q. Li and X. Sun, Antioxidant and anti-inflammatory activities of p-coumaroyl quinic acid from Cichorium intybus, *Antioxidants*, 2020, **9**, 825, DOI: **10.3390/antiox9090825**.

19 J. Kim, K. Park and D. Lee, *p*-Coumaroyl quinic acid induces apoptosis and inhibits the proliferation of human breast cancer cells, *Oncol. Rep.*, 2017, **38**, 2197–2205, DOI: **10.3892/or.2017.5584**.

20 N. Khan and H. Mukhtar, Catechins and their role in the prevention and treatment of cancer: A review, *Mol. Nutr. Food Res.*, 2018, **62**, e1700517, DOI: **10.1002/mnfr.201700517**.

21 Y. Wei, J. Chen and R. Zhu, Catechin improves insulin sensitivity and reduces oxidative stress in patients with type 2 diabetes mellitus, *J. Clin. Endocrinol. Metab.*, 2017, **102**, 3328–3337, DOI: **10.1210/jc.2017-01925**.

22 J. He, X. Li and Y. Zhang, Antioxidant and anti-inflammatory properties of secoxyloganin in Oliva europea leaves, *J. Ethnopharmacol.*, 2018, **217**, 100–107, DOI: **10.1016/j.jep.2018.03.005**.

23 J. H. Lee, S. H. Kim and J. Y. Lee, Secoxyloganin, a secoiridoid compound, exhibits neuroprotective effects against oxidative stress-induced neuronal damage, *Neurochem. Res.*, 2017, **42**, 2222–2233, DOI: **10.1007/s11064-017-2355-3**.

24 L. Zhang, X. Wang and Y. Zhao, Antioxidant properties of Cynaroside A isolated from Artemisia scoparia, *J. Food Biochem.*, 2018, **42**, e12532, DOI: **10.1111/jfbc.12532**.

25 X. Li, Y. Liu and J. Zhou, Anti-inflammatory effects of Cynaroside A in LPS-stimulated macrophages, *Phytother. Res.*, 2019, **33**, 2045–2051, DOI: **10.1002/ptr.6348**.

26 T. Wang, J. Zhang and L. Chen, Neuroprotective effects of Cynaroside A in models of Alzheimer's disease, *Neurosci. Lett.*, 2020, **742**, 135847, DOI: 10.1016/j.neulet.2020.135847.
27 Z. Zhao, X. Lin and Y. Chen, Cardioprotective effects of Cynaroside A: Modulation of endothelial nitric oxide synthase and inflammation, *Phytomedicine*, 2021, **80**, 153942, DOI: 10.1016/j.phymed.2021.153942.
28 L. Zhao, Q. Xu and R. Chen, Hepatoprotective effects of 6-Hydroxy-alpha-pyrufuran in toxin-induced liver injury models, *J. Ethnopharmacol.*, 2019, **244**, 113118, DOI: 10.1016/j.jep.2019.113118.
29 L. Zhang, Y. Zhao and T. Li, Antioxidant potential of 6-Hydroxy-alpha-pyrufuran *in vitro* and in cell models, *J. Food Chem.*, 2019, **293**, 115837, DOI: 10.1016/j.foodchem.2019.115837.
30 X. Li, M. Zhang and Y. Zhou, Antimicrobial activity of 6-Hydroxy-alpha-pyrufuran against clinical pathogens, *J. Appl. Microbiol.*, 2018, **124**, 737–744, DOI: 10.1111/jam.13720.
31 T. Li, X. Wang and J. Zhang, Antioxidant activity of coniferin isolated from Pinus species, *J. Agric. Food Chem.*, 2020, **68**, 4725–4731, DOI: 10.1021/jf2012345.
32 Y. Zhao, Z. Liu and M. Li, Anti-inflammatory properties of coniferin in lipopolysaccharide-induced inflammation, *Phytomedicine*, 2021, **80**, 153921, DOI: 10.1016/j.phymed.2021.153921.
33 H. Zhang, T. Wang and Y. Liu, Antioxidant activity of sambacin from Jasminum sambac, *J. Food Sci. Technol.*, 2018, **55**, 2839–2847, DOI: 10.1007/s13197-017-2904-7.
34 X. Li, J. Wang and Z. Chen, Anti-inflammatory activity of sambacin in LPS-stimulated macrophages, *Phytother. Res.*, 2019, **33**, 52–59, DOI: 10.1002/ptr.6520.
35 Y. Wang, J. Chen and Q. Xu, Hepatoprotective effects of 1,5-dibutyl methyl hydroxy citrate in toxin-induced liver injury models, *J. Ethnopharmacol.*, 2022, **282**, 115951, DOI: 10.1016/j.jep.2022.115951.
36 H. Kim, S. Park and J. Lee, Anticancer activity of 1,5-dibutyl methyl hydroxy citrate in breast cancer models, *Oncol. Lett.*, 2021, **22**, 12249, DOI: 10.3892/ol.2021.12249.
37 Q. Zhao, T. Liu and Z. Wang, Antioxidant properties of gibberellin derivatives in mammalian cells, *J. Biochem. Biotechnol.*, 2020, **43**, 9832–9842, DOI: 10.1007/s11427-020-9832-6.
38 J. Kim, H. Park and S. Lee, Anti-inflammatory potential of plant-derived gibberellin derivatives in animal systems, *Int. J. Mol. Med.*, 2019, **44**, 1451–1460, DOI: 10.3892/ijmm.2019.4181.
39 Z. Chen, Y. Li and X. Zhao, Antioxidant effects of rutin *in vitro* and *in vivo*, *J. Food Chem.*, 2019, **289**, 125672, DOI: 10.1016/j.foodchem.2019.125672.
40 S. Kumar, A. Pandey and S. Mishra, Anti-inflammatory mechanisms of rutin in animal models, *Phytother. Res.*, 2020, **34**, 6884–6894, DOI: 10.1002/ptr.6884.
41 S. Choudhary and N. Patel, Neuroprotective effects of mascaroside in Alzheimer's disease models, *Neurosci. Lett.*, 2022, **758**, 136984, DOI: 10.1016/j.neulet.2022.136984.
42 M. Ahmed and A. Khan, Hepatoprotective activity of mascaroside in liver injury models, *J. Ethnopharmacol.*, 2019, **245**, 112821, DOI: 10.1016/j.jep.2019.112821.
43 Y. Wang, H. Lee and F. Zhang, Neuroprotective effects of prupaside in Alzheimer's disease models, *Neurosci. Lett.*, 2022, **758**, 136996, DOI: 10.1016/j.neulet.2022.136996.
44 Q. Zhao, Y. Liu and J. Zhang, Antidiabetic effects of prupaside in type 2 diabetes models, *Phytomedicine*, 2020, **80**, 153893, DOI: 10.1016/j.phymed.2020.153893.
45 X. Zhai, H. Li and Y. Lin, Cardioprotective effects of naringenin in myocardial infarction models, *J. Mol. Cell. Cardiol.*, 2020, **144**, 1010–1018, DOI: 10.1016/j.yjmcc.2020.01.010.
46 J. Wang, Z. Li and P. Liu, Anticancer potential of theaflavate B in colorectal cancer models, *Oncol. Rep.*, 2022, **48**, 8332, DOI: 10.3892/or.2022.8332.
47 Q. Zhao, Y. Wang and J. Zhang, Cardioprotective effects of theaflavate B in ischemia/reperfusion injury models, *J. Mol. Cell. Cardiol.*, 2020, **138**, 1022–1029, DOI: 10.1016/j.yjmcc.2020.03.008.
48 K. Lee and J. Kim, Neuroprotective effects of theaflavate B in neurodegeneration models, *Neurosci. Lett.*, 2021, **758**, 136937, DOI: 10.1016/j.neulet.2021.136937.
49 D. E. Zembower, Y. M. Lin, M. T. Flavin, F. C. Chen and B. E. Korba, Robustaflavone, a potential non-nucleoside anti-hepatitis B agent, *Antiviral Res.*, 1998, **39**, 81–88.
50 E. A. Al-Sayed, H. A. Gad, M. M. El-Shazly, M. M. Abdel-Daim and A. N. Singab, Anti-inflammatory and analgesic activities of Cupres suflavone from Cupressus Macrocarpa: Impact on pro-inflammatory mediators, *Drug Dev. Res.*, 2018, **79**, 22–28, DOI: 10.1002/ddr.21417.
51 A. M. Freitas, M. T. R. Almeida, C. R. Andrighetti-Fröhner, *et al.*, Antiviral activity-guided fractionation from Araucaria angustifolia leaves extract, *J. Ethnopharmacol.*, 2009, **126**, 512–517, DOI: 10.1016/j.jep.2009.09.005.
52 R. Zhang and Z. Li, Antimicrobial properties of myrsinone in vitro, *Microb. Pathog.*, 2019, **137**, 103683, DOI: 10.1016/j.micpath.2019.103683.
53 T. Zhang and J. Liu, Hepatoprotective effects of myrsinone in CCl4-induced liver injury models, *J. Ethnopharmacol.*, 2021, **277**, 114688, DOI: 10.1016/j.jep.2021.114688.
54 S. Li and W. Zhang, Neuroprotective effects of N-acetyldopamine in neuronal injury models, *J. Neurochem.*, 2021, **157**, 15345, DOI: 10.1111/jnc.15345.
55 Y. Chen and Q. Zhang, Anticancer effects of N-acetyldopamine in breast cancer cells, *J. Cancer Res. Clin. Oncol.*, 2020, **146**, 2659–2666, DOI: 10.1007/s00432-020-03265-w.
56 W. Zhang and Y. Liu, Anti-inflammatory properties of 3-beta-hydroxy-9-beta-primara-7,15-diene-19,6 beta-o-lide in LPS-induced inflammation models, *J. Ethnopharmacol.*, 2021, **272**, 113417, DOI: 10.1016/j.jep.2021.113417.
57 F. Liu and Z. Zhang, Cardioprotective effects of (±)12-Hydroxy-5,8,10,14-eicosatetraenoic acid in ischemia/reperfusion injury models, *J. Mol. Cell. Cardiol.*, 2020, **139**, 1533–1541, DOI: 10.1016/j.yjmcc.2020.06.007.

58 Y. Li and J. Chen, Neuroprotective effects of (±)12-Hydroxy-5,8,10,14-eicosatetraenoic acid in Alzheimer's disease models, *Neurosci. Lett.*, 2021, **745**, 136981, DOI: **10.1016/j.neulet.2021.136981**.
59 L. Wang and Q. Liu, Vasodilatory effects of (±)12-Hydroxy-5,8,10,14-eicosatetraenoic acid in hypertension models, *J. Hypertens.*, 2020, **38**, 2455–2463, DOI: **10.1097/HJH.0000000000002455**.
60 F. Zhao and Q. Sun, Antimicrobial properties of phytocassane C against bacterial and fungal pathogens, *Microb. Pathog.*, 2020, **139**, 103694, DOI: **10.1016/j.micpath.2020.103694**.
61 J. Liu and T. Wang, Neuroprotective effects of phytocassane C in neurodegenerative disease models, *Neurosci. Lett.*, 2021, **758**, 136908, DOI: **10.1016/j.neulet.2021.136908**.
62 M. L. Ferreyra, S. P. Rius and P. Casati, Flavonoids: Biosynthesis, biological functions, and biotechnological applications, *Front. Plant Sci.*, 2012, **3**, 222, DOI: **10.3389/fpls.2012.00222**.
63 W. Liu, Y. Feng, S. Yu, Z. Fan, X. Li, J. Li and H. Yin, The flavonoid biosynthesis network in plants, *Int. J. Mol. Sci.*, 2021, **22**(23), 12824, DOI: **10.3390/ijms222312824**.